Nuclear Instruments and Methods in Physics Research A257 (1987) 91-96
North-Holland, Amsterdam

A SIMPLE METHOD FOR ENERGY CALIBRATION OF HEAVY-ION BEAMS

E.J. EVERS, J.W. DE VRIES, G.A.P. ENGELBERTINK and C. VAN DER LEUN

Fysisch Laboratorium, Rijksuniversiteit Utrecht, P.O. Box 80000, 3508 TA Utrecht, The Netherlands

Received 22 January 1987

A method is described for the calibration of analyzing-magnet systems of heavy-ion accelerators. It makes use of resonances in inverse (p, $\alpha\gamma$) reactions, i.e. with heavy-ion beams on hydrogen targets. Instead of a gas target we use the very thin hydrogen-containing surface layer on a gold foil, which makes the method very simple and applicable to almost any accelerator. The use of different charge states of the heavy-ion beam for the measurement of the same resonance provides internal consistency checks and makes it possible to cover a large energy range. The various contributions to the observed widths of the resonances used are briefly discussed. The resulting magnet calibration factor shows a linear decrease of about 0.2% over the range of 10–35 MeV equivalent proton energy. This calibration is used to determine an accurate energy, $E_p = (429.88 \pm 0.14)$ keV, for the well known narrow resonance in the reaction $^{15}N(p, \alpha\gamma)^{12}C$.

1. Introduction

During the last few years a remarkable revival has taken place of the interest in the $^{15}N(p, \alpha\gamma)^{12}C$ resonance at $E_p = 429$ keV and its equivalent in the inverse reaction $^{1}H(^{15}N, \alpha\gamma)^{12}C$ at $E(^{15}N) = 6.4$ MeV. The latter reaction is used for hydrogen profiling of solid materials [1–6], but also the nuclear resonance itself has been investigated in detail [6–9]. The most remarkable result is the new value for the resonance width. The 1982 review on the properties of $A = 16$ nuclei [10] gives a value equivalent to $\Gamma = 13$ keV (without error) in the inverse reaction, but at least three independent recent experiments yield values almost an order of magnitude smaller: $\Gamma = (1.9 \pm 0.2)$ keV [6], (1.8 ± 0.5) keV [7], and (1.55 ± 0.17) keV [8]. The last of these values is adopted in the most recent review [11]. This small width makes the resonance suitable for the investigation of other quantities such as the beam energy resolution and the contribution of the Doppler effect to the observed total width [9,12,13].

This paper discusses some of these effects, but concentrates on an accurate measurement of the resonance *energy* and on a simple but precise calibration method for analyzing-magnet systems of heavy-ion accelerators. The resonance energy is quoted in both the old and the new review with a relatively large error ($E_p = (429 \pm 1)$ keV) and has received very little attention in the recent work mentioned above.

Accelerator energy calibration based on nuclear resonances has been described before [14–16]. For proton energies above 4 MeV (p, n) threshold measurements are most frequently used [15,17–19]. Our method, which uses this narrow ($^{15}N + {}^{1}H$) and similar resonances, each with different charge states of the heavy-ion beam, and a very thin hydrocarbon contamination layer, well known from the profiling applications, as target, covers a wide energy range and is powerful because it provides internal consistency checks.

In sect. 2 some attention is paid to the conversion from the "classical" proton-capture reaction to the inverse reaction with a heavy-ion beam on a hydrogen target. Because of the high precision that can be achieved in this type of measurements the conversion should be handled with some care. Sect. 3 describes the experimental method, and sect. 4 presents the results on the resonance parameters and a discussion of the calibration method.

2. The inverse reaction

In laboratory situations A and B (see fig. 1) the energies available in the center of mass, E^A_{cm} and E^B_{cm} are relativistically given by

$$E_p = E^A_{cm}\left(\frac{m_p + M_{at}}{M_{at}} + \frac{E^A_{cm}}{2M_{at}c^2}\right), \tag{1}$$

and

$$E_{ion} = E^B_{cm}\left(\frac{M^{q+}_{ion} + m_H}{m_H} + \frac{E^B_{cm}}{2m_Hc^2}\right). \tag{2}$$

0168-9002/87/$03.50 © Elsevier Science Publishers B.V.
(North-Holland Physics Publishing Division)

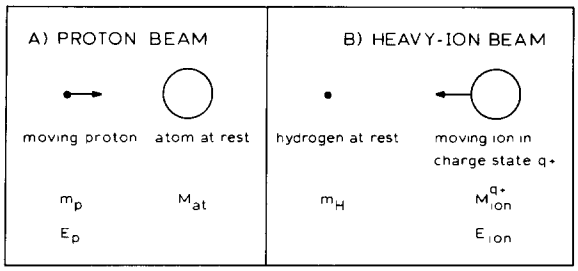

Fig. 1. The classical proton-beam system and the inverse reaction.

The condition $E_{cm}^{A} = E_{cm}^{B} = E_{cm}$ leads to the relation

$$\frac{E_{ion}}{E_p} = \frac{M_{at}}{m_H}\frac{M_{ion}^{q+} + m_H}{M_{at} + m_p} \times \frac{1 + E_{cm}/\left(2\left(M_{ion}^{q+} + m_H\right)c^2\right)}{1 + E_{cm}/\left(2\left(M_{at} + m_p\right)c^2\right)}. \tag{3}$$

The latter equation can be written as

$$\frac{E_{ion}}{E_p} = \frac{M_{at}}{m_H}(1 - \delta)(1 + \eta), \tag{4}$$

where δ and η are defined by

$$(1 - \delta) = \frac{M_{ion}^{q+} + m_H}{M_{at} + m_p}, \tag{4a}$$

and

$$(1 + \eta) = \frac{1 + E_{cm}/\left(2\left(M_{ion}^{q+} + m_H\right)c^2\right)}{1 + E_{cm}/\left(2\left(M_{at} + m_p\right)c^2\right)}. \tag{4b}$$

Neglect of the binding energies of the stripped electrons gives $m_p = m_H - m_e$ and $M_{ion}^{q+} = M_{at} - qm_e$ with m_e the electron mass. Eqs. (4a) and (4b) then result in

$$\delta = (q - 1)\frac{m_e}{M_{at} + m_p}, \tag{5}$$

and

$$\eta = \frac{E_{cm}}{2\left(M_{ion}^{q+} + m_H\right)c^2}\delta\frac{1}{1 + E_{cm}/\left(2\left(M_{at} + m_p\right)c^2\right)}. \tag{6}$$

The nonrestrictive limitations $M_{ion} > 4$ amu, $q < 10$, and $E_p < 5$ MeV result in $\delta < 10^{-3}$ and $\eta < 0.5 \times 10^{-6}$. The relativistic correction η is therefore negligible and, assuming $\eta = 0$, the ratio E_{ion}/E_p is calculated from eq. (4) with an accuracy better than 1 ppm. This ratio depends via δ very weakly on the charge state of the moving ion.

3. Experiment

3.1. Setup

Beams of ^{15}N and ^{19}F with $E = 6$–17 MeV and charge states 2^+–5^+ were obtained with a gas stripper from the Utrecht EN tandem. This accelerator has a double-focussing 90° analyzing magnet with a radius of curvature $\rho = 1$ m. For the measurements described here the slits at the object and image points of the magnet were set at a width $s = 1$ mm each and the slit currents were used as input to the stabilization system [20]. The well known formula for the resolution of an analyzing magnet, $\Delta E = Es/(2\rho)$, then leads to a beam energy spread limited to 0.05%. From the observed relation between the beam current and the slit width the actual beam energy spread was found to be (75 ± 15)% of this limiting value.

A schematic view of the target setup is given in fig. 2. The hydrogen-containing target was built up in-beam on a flat, 25 μm thick, Au foil, positioned in the small target chamber at an angle $\phi = 45°$ to the beam direction. To avoid disturbance of the measurement of the accumulated beam charge by secondary electrons, the beam current was integrated both at the target and at the surrounding insulated chamber.

Beam currents varied, depending on the beam ion and its charge state, from 20 to 100 nA (electrical) during the scans of the resonances and up to 230 nA during the buildup of the target (see sect. 3.2).

Two diaphragms were included in the setup. The first (with a diameter of 2 mm) collimated the beam. The second (diameter 2.5 mm) stopped beam ions scattered from the first diaphragm and, since it was kept at a constant potential of -170 V, formed a barrier for secondary electrons to enter or leave the target chamber, which would have disturbed the beam current measurement.

A liquid-nitrogen cooling trap was included just before the diaphragms, reducing the pressure in the target chamber to about 10^{-4} Pa (7×10^{-7} Torr).

The emitted γ-rays were detected in a 12.7 cm diameter NaI detector positioned at an angle $\theta = 90°$ to the

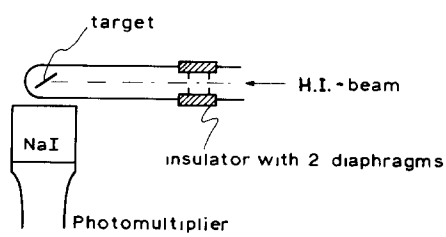

Fig. 2. Schematic view of the target setup.

beam direction at a distance $D = 2$ cm from the target spot. The NaI detector was shielded from the target with a 2 mm Pb foil to suppress X-rays and low-energy γ-rays.

3.2. Measuring procedure

3.2.1. Target stability

The target used was the hydrogen-containing contamination layer formed under beam impact on a clean Au foil in a 10^{-4} Pa vacuum. The stability of this layer is illustrated in fig. 3, which shows the 6.13–8.87 MeV γ-ray yield from the reaction $^{1}H(^{19}F, \alpha\gamma)^{16}O$ at the resonance energy $E(^{19}F) = 16.44$ MeV as a function of the accumulated dose of ^{19}F ions. This measurement was performed with a beam current of 230 nA $^{19}F^{3+}$, which means that the horizontal range displayed in fig. 3 corresponds to about one hour measuring time.

The very fast decrease at low dose is ascribed to the escape of water, the slow buildup to deposition of hydrocarbons originating from oil out of the vacuum pumps. From fig. 3 it is clear that already after a short time the layer becomes sufficiently stable to be used as a thin hydrogen target. The thickness at which the layer stabilizes has been reported to depend on the vacuum conditions [21].

3.2.2. Target thickness

The total observed width of a resonance yield curve is the quadratic sum of the intrinsic resonance width, the target thickness, the Doppler contribution due to the motion of the target atoms, and the energy resolution of the beam. This statement is strictly valid only if the various contributions to the observed width are all of Gaussian form. The Doppler contribution is indeed a Gaussian, the beam profile has a form between a Gaussian and a block, the target is assumed to have a block profile, and the resonance itself has a Lorentz shape. Hence care should be taken at this point. For a mixture of Gaussian and block profiles, the quadratic sum is a good approximation, provided that the total width of the block-form contribution is smaller than the sum of the widths of the Gaussian components. This condition is fulfilled for the measurements described here. However, for curves of Lorentzian shape a linear addition should be used. Whiting has reported a solution for the mixed case of a Gaussian and a Lorentzian contribution [22]:

$$\Gamma_{\text{Lorentz}} = \Gamma_{\text{observed}} - (\Gamma_{\text{Gauss}})^2/\Gamma_{\text{observed}}. \quad (7)$$

Fig. 4 displays two measurements of the ^{15}N resonance at $E(^{15}N^{2+}) = 6.4$ MeV where the angle between the beam direction and the target surfaces was 90° and $(22 \pm 4)°$ respectively. The only difference between these two measurements is a factor cos 68° in the target thickness. This measurement provided two values for the target thickness: $d = (2.5 \pm 0.8)$ keV from the shift in the energy with maximum yield, and $d = (3.7 \pm 0.9)$ keV from the difference in observed width, according to the quadratic addition mentioned above. The adopted weighted average, $d = (3.0 \pm 0.6)$ keV, leads to an actual contribution of $\Gamma_{\text{target}} = (4.3 \pm 0.8)$ keV in the further measurements, where the target was placed at an angle of 45°. With Ziegler's stopping powers [23] and the assumption that the composition of the layer is $(CH_2)_n$, this value corresponds to a thickness of almost 0.4 $\mu g/cm^2$.

3.2.3. Resonance curves

Resonance curves were taken by measuring the yield

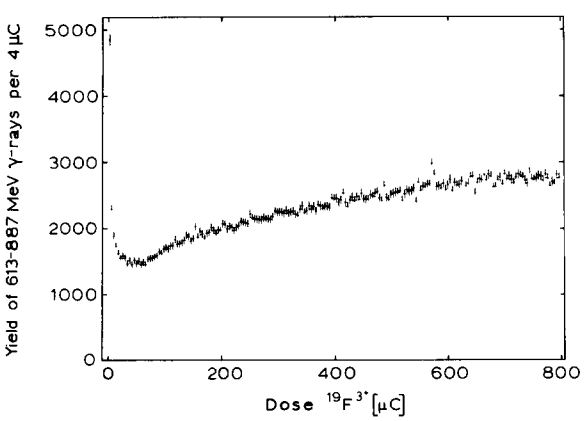

Fig. 3. Buildup of the hydrogen-containing surface layer as a function of the accumulated dose of ^{19}F ions.

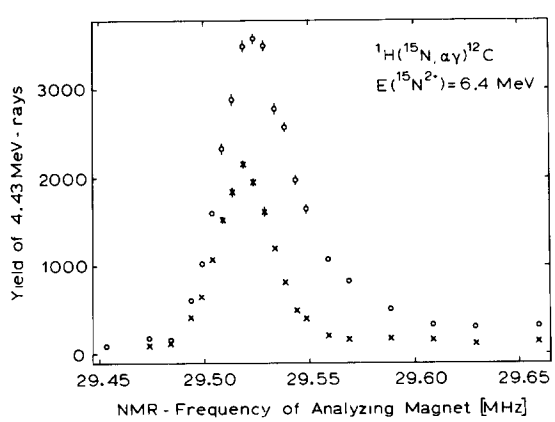

Fig. 4. Yield curves for the $^{1}H(^{15}N, \alpha\gamma)^{12}C$ resonance at $E(^{15}N^{2+}) = 6.4$ MeV that were used for the determination of the thickness of the surface layer. The angle between the beam direction and the target surface was 90° (×) and 22° (○) respectively.

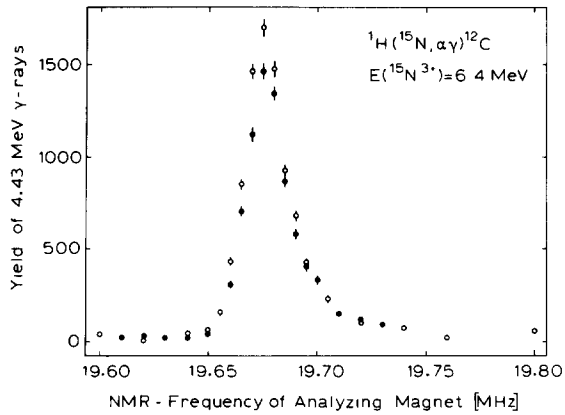

Fig. 5. Yield curves for the $^1H(^{15}N, \alpha\gamma)^{12}C$ resonance at $E(^{15}N^{3+}) = 6.4$ MeV, measured with increasing (black dots) and decreasing (open circles) magnetic field strength.

of the 4.43 MeV (for the ^{15}N resonances) and 6.13–8.87 MeV (for ^{19}F) γ-rays versus the field strength of the analyzing magnet. The magnetic field is determined with a nuclear magnetic resonance (NMR) probe and hence is given in terms of the NMR frequency f.

The resonance curves used for the determination of the resonance parameters were measured twice: once with increasing magnetic field strength (and hence increasing energy) and directly afterwards once again with decreasing field. This method provided a way to control effects of hysteresis and a second check on the stability of the target layer during the actual measurement. Examples of the measured resonance curves are displayed in figs. 5 and 6. The two frequencies thus obtained were generally found to agree within the errors and the weighted average was used.

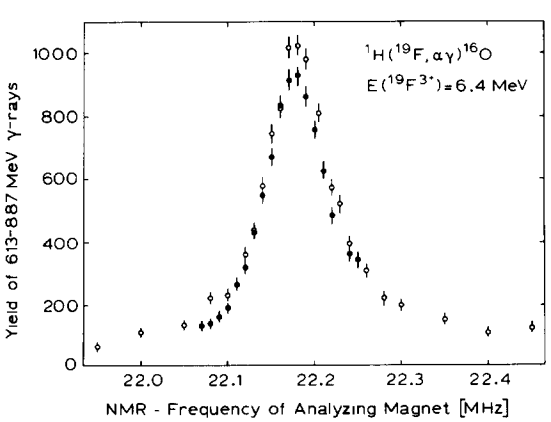

Fig. 6. Yield curves for the $^1H(^{19}F, \alpha\gamma)^{16}O$ resonance at $E(^{19}F^{3+}) = 6.4$ MeV, measured with increasing (black dots) and decreasing (open circles) magnetic field strength.

The complete final series of measurements used for the calibration was performed within one week. Several of the resonances, especially the narrow one at $E(^{15}N) = 6.4$ MeV, however, were measured repeatedly with consistent results.

4. Results and discussion

4.1. Resonance widths

The different contributions to the widths of the observed resonances are presented in table 1. All numbers are full widths at half maximum (fwhm). The observed widths are the weighted averages of the values obtained for each charge state used (see table 2). As described in sect. 3.2.2, the width due to the target thickness was measured for the narrow $E(^{15}N) = 6.4$ MeV resonance; the values for the other resonances were calculated from this value with Ziegler's stopping powers [23] under the assumption that the composition of the layer is $(CH_2)_n$. Since only ratios of two stopping power values are used in this calculation, the results are fairly independent of the absolute values given by Ziegler. Changing the target composition into $(CH_4)_n$ would affect the calculated values of the target thickness by less than 5%, whereas the experimental error is 20%. The energy resolution of the beam is calculated as described in sect. 3.1. The Doppler contributions are calculated from the fit to the experimental results given by Zinke–Allmang and Kalbitzer [13].

For all contributions except the intrinsic width, quadratic addition was used, as described in sect. 3.2.2. The intrinsic Lorentz widths were calculated with eq. (7). To enable comparison with the literature values [10,11,24], they were converted to the widths in the proton-beam system.

Although the present measurement did not primarily aim at accurate values for the resonance widths, the accuracy obtained warrants a comparison with literature data. The last two columns of table 1 indicate good agreement, except for the $E(p) = 897$ keV resonance, where the present result is somewhat smaller. For the $E(p) = 429$ keV resonance one could hardly expect good accuracy from the present method, since the intrinsic width is only a very small fraction of the observed width.

4.2. Energy calibration

The resonances used in the energy calibration are shown in table 2. The proton resonance energies are from Ajzenberg's reviews [10,11,24]. The heavy-ion resonance energies were calculated from these data with eq. (4)–(6) (see sect. 2) and the atomic masses from Wapstra and Audi [25]. Half of the target width was added to the

Table 1
Contributions to the observed widths of the four resonances [a)]

Ion	E_{res}(p) [b)]	$\Gamma_{observed}$(H.I.)	Γ_{target}(H.I.)	Γ_{beam}(H.I.)	$\Gamma_{Doppler}$(H.I.)	$\Gamma_{intrinsic}$(H.I.)	$\Gamma_{intrinsic}$(p) present	$\Gamma_{intrinsic}$(p) literature [b)]
^{19}F	872.11	93.0±2.8	5.2±1.0	6.2±1.2	21.7±0.3	87.2±3.0	4.63±0.16	4.7 ±0.2
^{19}F	340.46	53.0±2.6	5.8±1.2	2.4±0.5	13.6±0.2	48.8±2.8	2.59±0.15	2.4 ±0.2
^{15}N	897.37	31.7±0.9	3.6±0.7	5.0±1.0	17.4±0.3	21.0±1.3	1.41±0.09	1.70 ±0.15
^{15}N	429	13.5±0.6	4.2±0.8	2.4±0.5	12.0±0.2	1.1±1.3	0.07±0.09	0.103±0.011

[a)] All energies and widths are in keV. [b)] From refs. [11,24].

heavy-ion resonance energies to find the observed energies with maximum γ-ray yield. It should be noted that the other contributions to the observed width (as discussed in sect. 4.1) do *not* influence the calibration.

The results of the calibration of the analyzing magnet are displayed in fig. 7, which shows the calibration factor k as a function of the so-called "equivalent proton energy" E_p^{equi}. These quantities are defined by the relation

$$kf^2 = \frac{M_{ion}^{q+} E_{ion}}{q^2}\left(1 + \frac{E_{ion}}{2M_{ion}^{q+}c^2}\right)$$

$$= m_p E_p^{equi}\left(1 + \frac{E_p^{equi}}{2m_p c^2}\right). \quad (8)$$

The equivalent proton energy E_p^{equi}, the energy a proton should have to follow the same track through the magnet as the heavy ion, is independent of the charge state and mass of the heavy ion and is thus a direct measure for the magnetic field. The range E_p^{equi} = 10–35 MeV displayed in fig. 7 corresponds to a magnetic field range of about 0.45–0.85 T.

The line drawn in fig. 7 is a fit to the seven points with small errors. The two points from the $E(^{15}N) = 6.4$ MeV resonance were not included. These points would anyhow hardly influence the fit because of their large errors, which are caused by the large error in the proton resonance energy (see table 2). The line is described by

$$k[\text{keV amu/MHz}^2] = (27.5906 \pm 0.0031) - (2.40 \pm 0.12) \times 10^{-3} E_p^{equi}[\text{MeV}].$$

The points are very well described by this line (χ^2 = 0.2), but are clearly inconsistent with a constant magnet calibration factor (χ^2 = 13).

4.3. Energy of the narrow resonance in $^{15}N + {}^1H$

From the measured NMR frequencies at maximum γ-ray yield and the relation between the equivalent proton energy and the magnet calibration factor, new accurate values were calculated for the energy of the

Table 2
Data on the resonances used in the magnet calibration

p induced	H.I. induced				
E_{res} [a)] [keV]	Charge state	E_{res} [keV]	Shift due to target thickness [keV]	Frequency at maximum γ-ray yield [kHz]	"Equivalent proton energy" [b)] [MeV]
$^{19}F(^1H, \alpha\gamma)^{16}O$	$^1H(^{19}F, \alpha\gamma)^{16}O$				
872.11±0.20	3	16439.2±3.8	2.6±0.5	35528.7±1.3	34.46
	4	16438.7±3.8		26628.7±0.6	19.38
	5	16438.2±3.8		21295.1±1.0	12.40
340.46±0.04	2	6417.8±0.8	2.9±0.6	33293.3±1.0	30.28
	3	6417.6±0.8		22179.8±1.1	13.46
$^{15}N(^1H, \alpha\gamma)^{12}C$	$^1H(^{15}N, \alpha\gamma)^{12}C$				
897.37±0.29	3	13355.2±4.3	1.8±0.4	28437.0±0.7	22.10
	4	13354.8±4.3		21319.6±0.5	12.43
429 ±1	2	6385 ±15	2.1±0.4	29521.9±0.6	23.78
	3	6385 ±15		19676.2±0.3	10.57

[a)] From refs. [11,24]. [b)] See text.

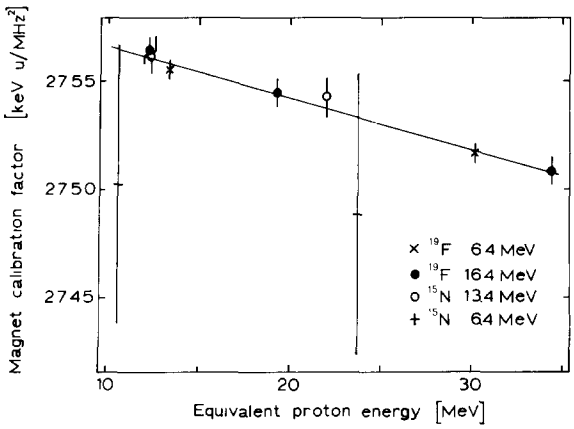

Fig. 7. Results for the magnet calibration factor (see text).

Table 3
Energy of the narrow ^{15}N resonance (in keV)

$^{15}N(^{1}H, \alpha\gamma)^{12}C$ ref. [11]	present	$^{1}H(^{15}N, \alpha\gamma)^{12}C$ calculated from present result
429 ± 1	429.88 ± 0.14	6398.0 ± 2.1 for charge state 2^+ 6397.8 ± 2.1 for charge state 3^+

$E_p = 429$ keV [11] resonance in ^{15}N(p, $\alpha\gamma$)^{12}C. The weighted average, calculated after conversion to the proton beam system, and the resulting resonance energies with a ^{15}N beam (for two charge states) are given in table 3.

To check the dependence of these values on the measured value of the target width, the calculation of the fit for the magnet calibration factor k as a function of the equivalent proton energy and the subsequent calculation of the resonance energies were repeated assuming the target width to be zero and twice the adopted value as described in sect. 3.2.2. The deviations thus found in the final value for the resonance energy were less than 20% of the error in this value. Hence, this result is not sensitive to the somewhat uncertain estimate of the target thickness.

5. Conclusion

A simple, fast, and accurate method is described for the calibration of analyzing-magnet systems of heavy-ion accelerators over a large energy range. It uses a mere gold foil as target and a standard NaI detector. The whole procedure can be accomplished within a few days, and the precision is limited mainly by the accuracy of the resonance energies used. Moreover, the method provides internal checks, since measurements of the same resonance with different charge states should yield consistent results.

The use of the accurate energy calibration in the determination of resonance energies is illustrated.

Acknowledgements

We thank Dr. C. Alderliesten for helpful discussions. This work was performed as part of the research program of the "Stichting voor Fundamenteel Onderzoek der Materie" (FOM) with financial support from the "Nederlandse Organisatie voor Zuiver Wetenschappelijk Onderzoek" (ZWO).

References

[1] W.A. Lanford, H.P. Trautvetter, J.F. Ziegler and J. Keller, Appl. Phys. Lett. 28 (1976) 566.
[2] W.A. Lanford, Nucl. Instr. and Meth. 149 (1978) 1.
[3] J.F. Ziegler et al., Nucl. Instr. and Meth. 149 (1978) 19.
[4] G. Amsel and B. Maurel, Nucl. Instr. and Meth. 218 (1983) 183.
[5] E.J. Evers and F.H.P.M. Habraken, Spectrochim. Acta 39B (1984) 1553.
[6] H. Damjantschitsch, M. Weiser, G. Heusser, S. Kalbitzer and H. Mannsperger, Nucl. Instr. and Meth. 218 (1983) 129.
[7] B. Maurel and G. Amsel, Nucl. Instr. and Meth. 218 (1983) 159.
[8] R.A. Leavitt, H.C. Evans, G.T. Ewan, H.-B. Mak, R.E. Azuma, C. Rolfs and K.P. Jackson, Nucl. Phys. A410 (1983) 93.
[9] G. Amsel, C. Cohen and B. Maurel, Nucl. Instr. and Meth. B14 (1986) 226.
[10] F. Ajzenberg-Selove, Nucl. Phys. A375 (1982) 1.
[11] F. Ajzenberg-Selove, Nucl. Phys. A460 (1986) 1.
[12] M. Zinke-Allmang, S. Kalbitzer and M. Weiser, Z. Phys. A320 (1985) 697.
[13] M. Zinke-Allmang and S. Kalbitzer, Z. Phys. A323 (1986) 251.
[14] R.O. Bondelid and C.A. Kennedy, Phys. Rev. 115 (1959) 1601.
[15] J.B. Marion, Rev. Mod. Phys. 38 (1966) 660.
[16] H.P. Trautvetter, K. Elix, C. Rolfs and K. Brand, Nucl. Instr. and Meth. 161 (1979) 173.
[17] J.C. Overley, P.D. Parker and D.A. Bromley, Nucl. Instr. and Meth. 68 (1969) 61.
[18] R.E. White, Nucl. Instr. and Meth. 160 (1979) 199.
[19] J.F. Wilkerson, T.B. Clegg and E.J. Ludwig, Nucl. Instr. and Meth. 207 (1983) 331.
[20] A. Vermeer and B.A. Strasters, Nucl. Instr. and Meth. 157 (1978) 427.
[21] J.-P. Thomas, M. Fallavier and J. Tousset, Nucl. Instr. and Meth. 187 (1981) 573.
[22] E.E. Whiting, J. Quant. Spectrosc. Radiat. Transfer 8 (1968) 1379.
[23] J.F. Ziegler, Handbook of stopping cross-sections for energetic ions in all elements (Pergamon, New York, 1980).
[24] F. Ajzenberg-Selove, Nucl. Phys. A392 (1983) 1.
[25] A.H. Wapstra and G. Audi, Nucl. Phys. A432 (1985) 1.